Radiology

ORIGINAL RESEARCH • NEURORADIOLOGY

Comparison of Multivendor Single-Voxel MR Spectroscopy Data Acquired in Healthy Brain at 26 Sites

Michal Považan, PhD • Mark Mikkelsen, PhD • Adam Berrington, PhD • Pallab K. Bhattacharyya, PhD • Maiken K. Brix, MD • Pieter F. Buur, PhD • Kim M. Cecil, PhD • Kimberly L. Chan, PhD • David Y.T. Chen, MD • Alexander R. Craven, MS • Koen Cuypers, PhD • Michael Dacko, PhD • Niall W. Duncan, PhD • Ulrike Dydak, PhD • David A. Edmondson, PhD • Gabriele Ende, PhD • Lars Ersland, PhD • Megan A. Forbes, PhD • Fei Gao, PhD • Ian Greenhouse, PhD • For the Group[1]

From the Division of Neuroradiology, Park 367B, Russell H. Morgan Department of Radiology and Radiological Science, The Johns Hopkins University School of Medicine, 600 N Wolfe St, Baltimore, MD 21287 (M.P., M.M., A.B., K.L.C., G.O., N.A.J.P., M.G.S., R.A.E.E., P.B.B.); F.M. Kirby Research Center for Functional Brain Imaging, Kennedy Krieger Institute, Baltimore, MD (M.P., M.M., A.B., K.L.C., G.O., N.A.J.P., M.G.S., R.A.E.E., P.B.B.); Imaging Institute, Cleveland Clinic Foundation, Cleveland, OH (P.K.B.); Department of Radiology, Cleveland Clinic Lerner College of Medicine of Case Western Reserve University, Cleveland, OH (P.K.B.); Department of Radiology, Haukeland University Hospital, Bergen, Norway (M.K.B.); Spinoza Centre for Neuroimaging, Amsterdam, the Netherlands (P.F.B., D.S.); Department of Radiology, Cincinnati Children's Hospital Medical Center, Cincinnati, OH (K.M.C.); Department of Biomedical Engineering, The Johns Hopkins University School of Medicine, Baltimore, MD (K.L.C.); Department of Radiology, Taipei Medical University Shuang Ho Hospital, New Taipei City, Taiwan (D.Y.T.C.); Department of Biological and Medical Psychology, University of Bergen, Bergen, Norway (A.R.C., L.E.); NOreMENT–Norwegian Center for Mental Disorders Research, University of Bergen, Bergen, Norway (A.R.C., L.E.); Movement Control & Neuroplasticity Research Group, Department of Movement Sciences, Group of Biomedical Sciences, KU Leuven, Leuven, Belgium (K.C., C.M., S.P.S.); REVAL Rehabilitation Research Center, Hasselt University, Diepenbeek, Belgium (K.C.); Department of Radiology, Medical Physics, Medical Center-University of Freiburg, Faculty of Medicine, University of Freiburg, Freiburg, Germany (M.D., T.L.); Brain and Consciousness Research Centre, Taipei Medical University, Taipei, Taiwan (N.W.D.); School of Health Sciences, Purdue University, West Lafayette, IN (U.D., D.A.E., R.M.); Department of Radiology and Imaging Sciences, Indiana University School of Medicine, Indianapolis, IN (U.D., D.A.E.); Department of Neuroimaging, Central Institute of Mental Health, Mannheim, Germany (G.E., M.S.); Department of Clinical Engineering, Haukeland University Hospital, Bergen, Norway (A.R.C., L.E.); Department of Clinical and Health Psychology, University of Florida, Gainesville, FL (M.A.F., E.C.P., A.J.W.); Center for Cognitive Aging and Memory, McKnight Brain Institute, University of Florida, Gainesville, FL (M.A.F., E.C.P., A.J.W.); Shandong Medical Imaging Research Institute, Shandong University, Jinan, China (F.G., G.W.); Department of Human Physiology, University of Oregon, Eugene, OR (I.G.). Received May 17, 2019; revision requested July 29; revision received November 14; accepted November 25. **Address correspondence to** P.B.B. (e-mail: *pbarker2@jhmi.edu*).

Supported by the National Institutes of Health (NIH) (R01 EB016089, R01 EB023963, P41 EB015909). Data acquisition was supported by Taiwan Ministry of Science and Technology (105-2410-H-038-006-MY3). Data collection was supported by the Shandong Provincial Key Research and Development Plan of China (2016ZDJS07A16), National Natural Science Foundation of China for Young Scholars (81601479), and Taishan Scholars Project (tsqn201812147).

A.J.W. was supported by the National Institute on Aging (K01 AG050707, R01 AG054077), University of Florida (UF), Center for Cognitive Aging and Memory (CAM), and McKnight Brain Research Foundation (MBRF). D.A.E. was supported by NIH (F31 ES028081). E.C.P. was supported by the National Institute on Alcohol Abuse and Alcoholism (NIAAA) (K01 AA025306), UF, CAM, and MBRF. H.J.Z. was supported by Deutsche Forschungsgemeinschaft (SFB 974 TP B07). J.J.P. was supported by NIAAA (K23 AA020842). K.M.C. was supported by NIH (R01 MH095014, R01 NS096207). M.P.S. was supported by NIH (F32 EY025121). N.A.J.P. receives salary support from NIH (R00 MH107719). S.P.S. supported by Research Foundation-Flanders (G089818N), Excellence of Science (30446199, MEMODYN [The Journey of a Memory: Dynamics of Learning and Consolidation in Maturation and Aging]), and the KU Leuven Research Fund (C16/15/070).

[1] The complete list of authors and affiliations is at the end of this article.

Conflicts of interest are listed at the end of this article.

Radiology 2020; 295:171–180 • https://doi.org/10.1148/radiol.2020191037 • Content codes: MR NR

Background: The hardware and software differences between MR vendors and individual sites influence the quantification of MR spectroscopy data. An analysis of a large data set may help to better understand sources of the total variance in quantified metabolite levels.

Purpose: To compare multisite quantitative brain MR spectroscopy data acquired in healthy participants at 26 sites by using the vendor-supplied single-voxel point-resolved spectroscopy (PRESS) sequence.

Materials and Methods: An MR spectroscopy protocol to acquire short-echo-time PRESS data from the midparietal region of the brain was disseminated to 26 research sites operating 3.0-T MR scanners from three different vendors. In this prospective study, healthy participants were scanned between July 2016 and December 2017. Data were analyzed by using software with simulated basis sets customized for each vendor implementation. The proportion of total variance attributed to vendor-, site-, and participant-related effects was estimated by using a linear mixed-effects model. *P* values were derived through parametric bootstrapping of the linear mixed-effects models (denoted P_{boot}).

Results: In total, 296 participants (mean age, 26 years ± 4.6; 155 women and 141 men) were scanned. Good-quality data were recorded from all sites, as evidenced by a consistent linewidth of *N*-acetylaspartate (range, 4.4–5.0 Hz), signal-to-noise ratio (range, 174–289), and low Cramér-Rao lower bounds (≤5%) for all of the major metabolites. Among the major metabolites, no vendor effects were found for levels of myo-inositol ($P_{boot} > .90$), *N*-acetylaspartate and *N*-acetylaspartylglutamate ($P_{boot} = .13$), or glutamate and glutamine ($P_{boot} = .11$). Among the smaller resonances, no vendor effects were found for ascorbate ($P_{boot} = .08$), aspartate ($P_{boot} > .90$), glutathione ($P_{boot} > .90$), or lactate ($P_{boot} = .28$).

Conclusion: Multisite multivendor single-voxel MR spectroscopy studies performed at 3.0 T can yield results that are coherent across vendors, provided that vendor differences in pulse sequence implementation are accounted for in data analysis. However, the site-related effects on variability were more profound and suggest the need for further standardization of spectroscopic protocols.

Online supplemental material is available for this article.

Abbreviations

CRLB = Cramér-Rao lower bounds, Glx = glutamate and glutamine, mI = myo-inositol, NAA = *N*-acetylaspartate, PRESS = point-resolved spectroscopy, SNR = signal-to-noise ratio, tCr = total creatine

Summary

In a multisite study of brain MR spectroscopy performed at 26 sites, interindividual differences were found as the main contributor to variability, demonstrating that appropriately analyzed MR spectroscopy data acquired at different sites and with different scanners can be compared.

Key Results

- Short-echo-time MR spectroscopy of the human brain performed at 3.0 T quantifies eight metabolites (*N*-acetylaspartate and *N*-acetylaspartylglutamate [total NAA], glycerophosphocholine and phosphocholine, creatine and phosphocreatine, myo-inositol [mI], glutamate and glutamine [Glx], glucose and taurine, gluthathione, aspartate) in all participants based on the defined quality exclusion criteria in a 27-mL voxel and approximately 2-minute acquisition time.
- All MR spectra showed a consistent linewidth of *N*-acetylaspartate (range, 4.4–5.0 Hz), signal-to-noise ratio (range, 174–289), and low Cramér-Rao lower bounds (≤5%) for total NAA, glycerophosphocholine and phosphocholine, creatine and phosphocreatine, mI, and Glx.
- The vendor contribution to total variance of metabolite levels ranged from 0% to 27%. *P* values were derived through parametric bootstrapping of the linear mixed-effects models (denoted as P_{boot}). No vendor effects were found for levels of mI ($P_{boot} > .90$), total NAA ($P_{boot} = .13$), Glx ($P_{boot} = .11$), ascorbate ($P_{boot} = .08$), aspartate ($P_{boot} > .90$), glutathione ($P_{boot} > .90$), and lactate ($P_{boot} = .28$). The site-related effects ranged from 3% up to 44% and the remaining 50%–83% of the total variance was accounted for by interindividual differences, which included both actual biologic differences as well as within-participant measurement error.

Single-voxel proton (hydrogen 1 [^{1}H]) MR spectroscopy gives useful information for both clinical diagnosis and research studies (1,2) and is commercially available with most MRI scanners at 1.5 T and 3.0 T. The point-resolved spectroscopy (PRESS) sequence (3) is most widely used for brain MR spectroscopy because it provides robust results from well-defined regions of interest. However, implementations of the sequence are diverse among manufacturers and research sites. They differ in terms of timing and waveforms of the radiofrequency pulses, as well as water suppression and preparation methods, all of which may influence quantification. While recent efforts have focused on standardization of single-voxel MR spectroscopy methods between vendors, including the use of advanced localization sequences such as semi-localized by adiabatic selective refocusing (4,5), currently most clinical MR spectroscopy studies continue to use the manufacturer-supplied PRESS sequence.

At 3.0 T, conventional MR spectroscopy can reliably detect the signals of *N*-acetylaspartate (NAA) and *N*-acetylaspartylglutamate (total NAA), total choline (glycerophosphocholine and phosphocholine), total creatine (tCr) (creatine and phosphocreatine), myo-inositol (mI), and glutamate and glutamine (Glx). These metabolites are commonly known as major metabolites. In addition, a variable number of less abundant minor metabolites are often reported, based on the spectral quality and the defined exclusion criteria.

Recently, a large study involving almost 300 healthy participants at multiple sites was performed, investigating the reliability of the measurement of brain γ-aminobutyric acid levels by using the Mescher-Garwood (MEGA)-PRESS (6) spectral editing technique (7,8). As a second part of that study, conventional short-echo-time MR spectroscopy data were also collected by using the vendor-supplied PRESS sequence. The current study reports on the results of the analysis of these single-voxel PRESS data, which could have important implications for the design of multisite studies using MR spectroscopy as an outcome measure, as well as for comparing clinical or research results in individual participants performed with different scanners.

The purpose of our study, therefore, was to compare multisite quantitative brain MR spectroscopy data acquired in healthy participants at 26 sites by using the vendor-supplied single-voxel PRESS sequence.

Materials and Methods

Study Participants

All data in our prospective study were acquired between July 2016 and December 2017. Institutional review board approval and participant written informed consent were obtained at each site. Participants were recruited with the following inclusion criteria: age between 18–35 years, no known neurologic illness, and medication free without usage of over-the-counter pain relievers or allergy medication in the preceding 36 hours. Anonymized data were analyzed at the Johns Hopkins University (Baltimore, Md). As stated previously, participants' brain γ-aminobutyric acid levels recorded by using a spectral editing sequence were previously reported in the literature (7,8). This study reports levels of metabolites collected by using conventional PRESS sequence.

Data Acquisition

Each site acquired vendor-specific ^{1}H MR spectroscopy PRESS data with a 3.0-T scanner using phased-array radiofrequency head coils. Eight sites were equipped with GE scanners (GE Healthcare, Chicago, Ill), 10 with Philips scanners (Philips Healthcare, Best, the Netherlands), and eight with Siemens scanners (Siemens Healthineers, Erlangen, Germany) (Table E1 [online]). Three-dimensional T1-weighted images were acquired to position a 30 × 30 × 30 mm^3 MR spectroscopy voxel in the medial parietal lobe (Fig 1). The ^{1}H MR spectroscopy data were measured with the following parameters: repetition time, 2000 msec; echo time, 35 msec; number of averages, 64; spectral bandwidth, 2 kHz or 4 kHz or 5 kHz; data points, 2048 or 4096; scan time, 2 minutes 8 seconds. Water reference scans were acquired for coil combination and eddy current correction with similar parameters and 8 or 16 averages. No other MR acquisition parameters were specified to participating sites. Therefore, additional acquisition-related methodology including the methods for main magnetic field (B_0) homogeneity adjustment, phase cycling scheme, water suppression, and outer volume suppression varied from site to site according to local preferences and availability. The ^{1}H MR spectroscopy data were saved as P-files (GE), SDAT/SPAR files

(Philips), or TWIX files (Siemens). An overview of hardware and software parameters is provided in Table E1 (online).

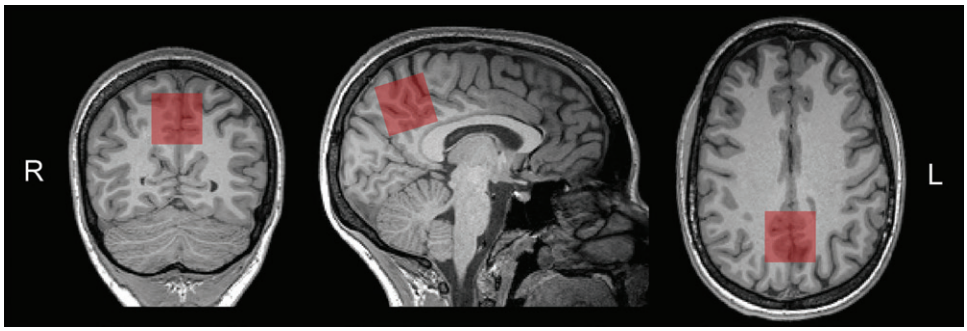

Figure 1: Image shows example of 30 × 30 × 30 mm^3 spectroscopic voxel placement on T1-weighted image. Voxel was rotated in sagittal plane to be parallel with line connecting genu and splenium of corpus callosum. L = left, R = right.

Data Quantification

Data were processed by a medical physicist (M.P., with 7 years of experience) by using automated in-house Matlab-based (MathWorks, Natick, Mass) software (9) with the FID-A toolkit (10). Results were evaluated in consensus with all coauthors. Raw data (GE and Siemens) were coil combined using water reference (11) and eddy current corrected, frequency corrected, and phase corrected (12). Subsequently, spectra were quantified by using LCModel (version 6.3–0D; Stephen Provencher, Oakville, Canada) (13) over the frequency range from 0.5 ppm to 4.0 ppm. Basis sets consisted of 19 metabolites: alanine, ascorbate, aspartate, creatine, γ-aminobutyric acid, glucose, glutamine, glutamate, glutathione, glycerophosphocholine, lactate, mI, NAA, *N*-acetylaspartylglutamate, phosphocholine, phosphocreatine, phosphoethanolamine, scyllo-inositol, and taurine. Metabolite basis spectra were generated by using custom-built fully localized two-dimensional density matrix simulations and vendor-native shaped refocusing pulse information and phase cycling (14). Chemical shifts and scalar coupling *(J)* constants from Tkáč et al (15) were used for all metabolites except for NAA, *N*-acetylaspartylglutamate, glutamate, and glutamine, which used values from Govind and colleagues (16). Macromolecules were modeled in LCModel (Appendix E1 [online]). Four vendor-specific basis sets were used to fit the data (two for GE [due to different sequence timings], one for Philips, and one for Siemens).

All spectra were visually inspected to detect any spurious artifacts or lipid contamination. A spectrum was excluded from further analysis if the lipid peak amplitude was higher than the amplitude of the NAA singlet (-CH_3 group at 2.008 ppm).

Quantified values were processed based on quality criteria as described by Tkáč and colleagues (17). Metabolite values with Cramér-Rao lower bounds (CRLB) above 100% were excluded. If a specific metabolite did not have CRLBs less than 100% in at least 50% (147 of 293) of the quantified spectra, then it was excluded from further analysis. Finally, a metabolite was also excluded if it had average CRLBs higher than 50%. Signal-to-noise ratio (SNR) was calculated as a ratio of NAA signal intensity divided by a standard deviation of noise. Linewidth was calculated as a full width at half maximum of the NAA peak.

The relative concentration of metabolites was calculated as a ratio to tCr.

Participant Demographic Data by Site

Site Identifier	Sample Size	Age (y)*	Sex†
G1	12	23.9 ± 4.8	7/5
G2	12	26.8 ± 4.0	6/6
G3	7	23.4 ± 5.5	2/5
G4	12	25.6 ± 4.5	6/6
G5	12	25.5 ± 3.7	5/7
G6	12	24.3 ± 4.2	6/6
G7	12	28.1 ± 4.0	6/6
G8	12	29.7 ± 2.1	6/6
All GE	91	26.1 ± 4.4	44/47
P1	12	25.1 ± 3.2	6/6
P2	12	28.8 ± 3.9	10/2
P3	12	29.3 ± 3.1	5/7
P4	12	24.9 ± 4.3	7/5
P5	8	23.1 ± 2.4	3/5
P6	12	27.3 ± 3.7	7/5
P7	12	23.3 ± 2.0	6/6
P8	12	23.6 ± 3.7	5/7
P9	12	25.8 ± 4.6	6/6
P10	12	25.1 ± 2.9	6/6
All Philips	116	25.7 ± 4.0	61/55
S1	12	25.7 ± 3.7	6/6
S2	5	40.4 ± 7.4	0/5
S3	12	31.6 ± 3.4	9/3
S4	12	27.7 ± 2.8	6/6
S5	12	26.5 ± 3.7	6/6
S6	12	24.9 ± 2.0	6/6
S7	12	28.8 ± 3.8	6/6
S8	12	24.0 ± 3.5	11/1
All Siemens	89	27.8 ± 5.2	50/39
Total	296	26.4 ± 4.6	155/141

Note.—GX = GE Healthcare (Chicago, IL) sites, PX = Philips Healthcare (Best, the Netherlands) sites, SX = Siemens Healthineers (Erlangen, Germany) sites.

* Data are means ± standard deviation.

† Numerators are the number of women, and denominators are the number of men.

Statistical Analysis

Linear mixed-effects models were fit to the metabolite data in R (version 3.5.3; R Foundation, Vienna, Austria [18]) (M.M. [neuroscientist with 12 years of experience with statistics]). An unconditional model (Equation 1 in Mikkelsen et al [7]) was fitted to calculate variance partition coefficients to estimate the proportion of total variance attributed to vendor-, site-, and participant-related effects. Secondary, conditional

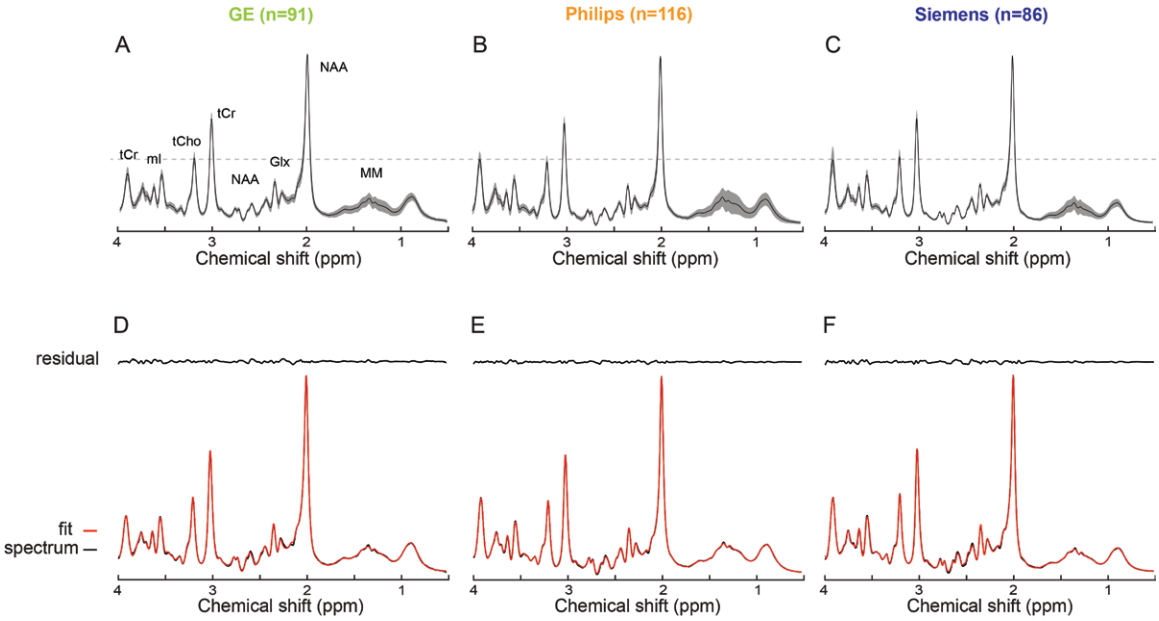

Figure 2: Graphs show average spectra from, *A*, GE Healthcare (Chicago, IL), *B*, Philips Healthcare (Best, the Netherlands), and, *C*, Siemens Healthineers (Erlangen, Germany) scanners with gray areas representing ± 1 standard deviation. Average LCModel (version 6.3–0D; Stephen Provencher, Oakville, Canada) fit results (red) and average residuals are shown for, *D*, the GE, *E*, the Philips, and, *F*, the Siemens scanners. Dashed line illustrates difference in methylene peak of creatine and phosphocreatine at 3.9 ppm that was partially suppressed by water suppression. Glx = glutamate and glutamine, NAA = *N*-acetylaspartate, mI = myo-inositol, MM = macromolecules, tCho = total choline, tCr = total creatine.

linear mixed-effects models (Equation 5 in Mikkelsen et al [7]) were also fitted to assess the impact of SNR, linewidth, age, and sex on quantified measurements. Goodness of fit was calculated as a log-likelihood statistic. Parametric bootstrapping was then used whereby the null distributions of each test was simulated by bootstrapping the fitted distributions (2000 simulations) to evaluate the probability of observing the test statistics given the distribution of the null hypotheses (19). *P* values are denoted P_{boot}.

Effects that were tested included vendor and site, SNR and linewidth, and age and sex. Posthoc pairwise comparisons were corrected for multiple comparisons by using the Holm-Bonferroni method (20). *P* values are denoted P_{Holm}. An adjusted *P* value less than .05 was considered to indicate statistical significance.

Results

Study Participants

Twenty-six research sites participated in our study, with each site contributing up to 12 data sets. In total, data from 296 healthy participants were collected (155 women and 141 men; mean age ± standard deviation, 26 years ± 4.6; age inclusion range, 18–35 years). After visual inspection, three participants (examined by using Siemens scanners) were removed from further analysis due to lipid contamination. There were no differences in sex ($P = .69$) of participants between the groups examined by using scanners from the different vendors. Participants examined by using Siemens scanners were older by approximately 2 years compared with those examined at GE ($P_{Holm} = .03$) and Philips ($P_{Holm} = .005$) sites. Demographic information on participants is given in the Table.

Data Quantification

Mean PRESS spectra are displayed in Figure 2, *A–C,* for each vendor. Qualitatively, spectral profiles were in very good agreement across vendors. The creatine and phosphocreatine peak of 3.9 ppm was consistently lower for data acquired by using GE scanners compared with the other two vendors due to higher bandwidth of the water suppression pulses (Figure 2, *A–C*; dashed line). Figure 2, *D–F,* shows vendor-specific mean fits and residuals from the LCModel fitting routine. An example of a quantified spectrum with fitted basis spectra of metabolites and macromolecules is shown in Figure 3.

The overall high quality of the data is reflected in high SNR and narrow linewidth values. Vendor-specific mean SNR ± standard deviation for GE, Philips, and Siemens scanners were 174.3 ± 37.4, 196.3 ± 52.9, and 288.8 ± 80.6, respectively. Vendor-specific mean linewidth of NAA for GE, Philips, and Siemens was 5.0 Hz ± 0.8, 4.6 Hz ± 1.0, and 4.4 Hz ± 0.6, respectively. The individual site and vendor SNR and linewidth values are shown in Figure E1 (online). SNR values of data acquired by using Siemens scanners was higher than were SNR values acquired by using GE and Philips scanners (both $P_{Holm} < .001$). SNR values were not different between data acquired by using GE and Philips scanners ($P_{Holm} = .35$). There were no differences in linewidth between the data acquired by using scanners from the different vendors: GE versus Philips, $P_{Holm} = .29$; GE versus Siemens, $P_{Holm} = .06$; Philips versus Siemens, $P_{Holm} = .32$.

Based on the correlation matrix provided by LCModel (ie, mean correlation coefficient for a metabolite pair less than −0.3), sums of metabolites are reported for total NAA, tCr (creatine and phosphocreatine), glycerophosphocholine and

phosphocholine (total choline), and taurine and glucose. Also, due to substantial spectral overlap of glutamate and glutamine (Glx) at 3.0 T, only their summed values (ie, Glx) are reported (21). Thus, 14 metabolites or metabolite sums were quantified. Mean CRLB of alanine was above 50% and was therefore excluded from further analysis. Eight metabolites were quantified in all participants, scyllo-inositol in 99.0% (290 of 293), phosphoethanolamine in 98.0% (287 of 293), γ-aminobutyric acid in 95.9% (281 of 293), lactate in 94.9% (278 of 293), and ascorbate in 81.9% (240 of 293) of all participants (Table E2 [online]).

Metabolite ratios relative to tCr and their relative CRLBs are listed in Tables E3 and E4 (online), and vendor-specific mean metabolite ratios compared by site are shown in Figure 4. CRLBs were below 2% for tCr and total NAA and below 5% for total choline, mI, and Glx across all sites and vendors (Table E4 [online]). Eleven of 13 metabolites acquired with Siemens scanners, 10 of 13 metabolites acquired with Philips scanners, and eight of 13 metabolites acquired with GE scanners had site-specific mean and vendor-specific mean CRLBs below 20%.

Mean between-participant coefficients of variation (Table E5 [online]) and intersite coefficients of variation (Table E2 [online]) were below 10% for total choline/tCr, total NAA/tCr, Glx/tCr, and mI/tCr. Between-participant coefficients of variation are compared against site-mean CRLBs in Figure 5. Four major metabolite ratios (total choline/tCr, Glx/tCr, mI/tCr, and total NAA/tCr) showed substantially lower CRLBs (in the range of 1%–5%) compared with their corresponding between-participant coefficients of variation (range of 4%–15%).

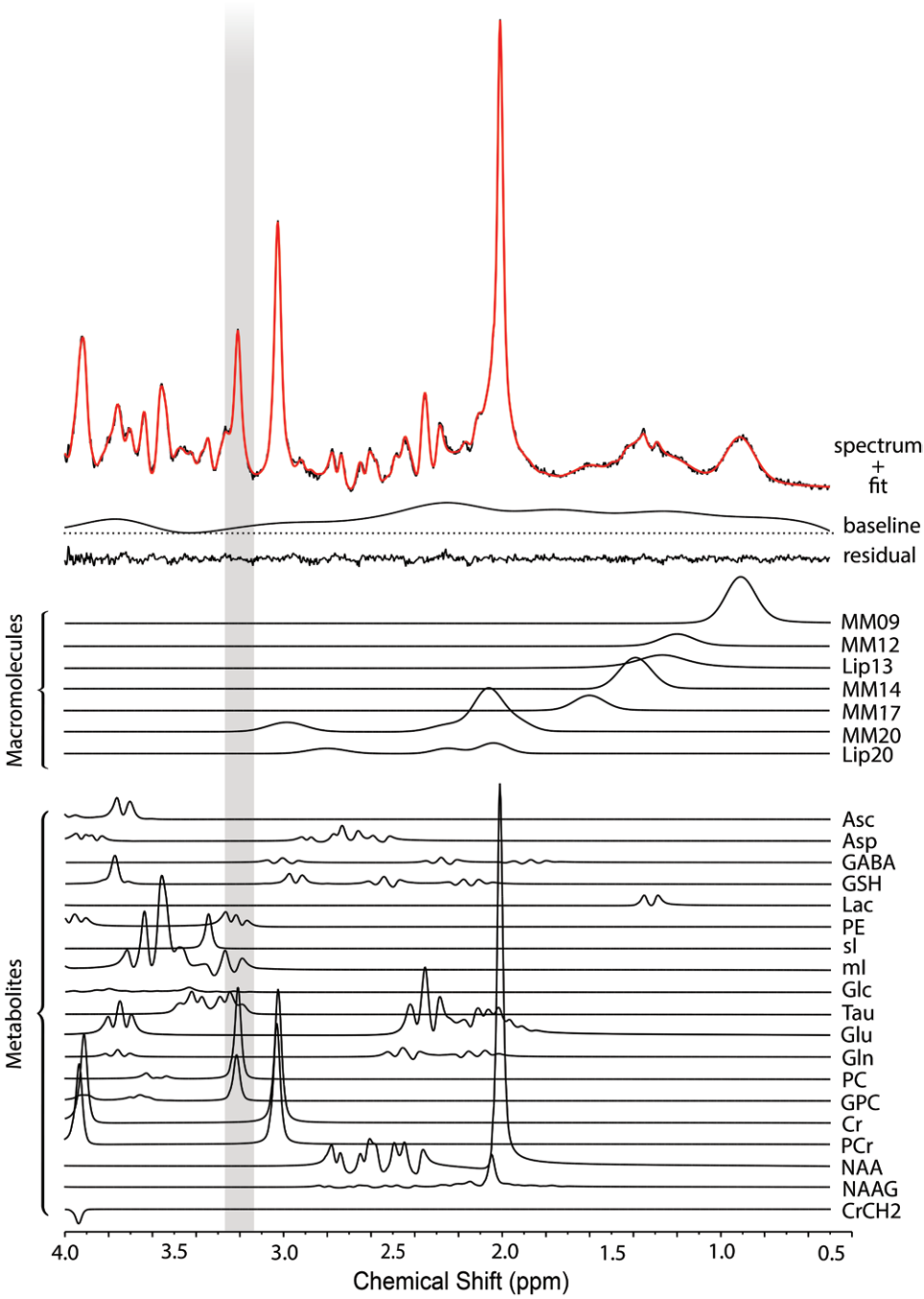

Figure 3: Image shows example LCModel (version 6.3–0D; Stephen Provencher, Oakville, Canada) analysis with one spectrum, LCModel fit (red), spline baseline, residual, and individual macromolecule and metabolite contributions. Gray band highlights spectral region approximately 3.2 ppm, where signals of phosphoethanolamine (PE), myo-inositol (mI), glucose (Glc), taurine (Tau), glycerophosphocholine (GPC), and phosphocholine (PC) substantially overlap. Spectral fitting algorithm based on linear combination of model spectra as used in this study may be affected by this spectral overlap. This may introduce additional variability that is reflected on vendor level. Asc = ascorbate, Asp = aspartate, Cr = creatine, GABA = γ-aminobutyric acid, Gln = glutamine, Glu = glutamate, GSH = glutathione, Lac = lactate, NAA = *N*-acetylaspartate, NAAG = *N*-acetylaspartylglutamate, PCr = phosphocreatine, sI = scyllo-inositol, CrCH2 = correction term for Cr, MM09 = macromolecule peak at 0.9 ppm, MM12 = macromolecule peak at 1.2 ppm, MM14 = macromolecule peak at 1.4 ppm, MM17 = macromolecule peak at 1.7 ppm, MM20 = macromolecule peaks at 2.0 ppm and 3.0 ppm, Lip13 = lipid peak at 1.3 ppm, Lip20 = lipid peaks at 2.0 ppm and 2.2 ppm and 2.8 ppm.

Statistical Analysis

The vendor contribution to the total variance of the metabolite concentrations ranged from 0% to 27%. The site-related effects were more pronounced and found for all but

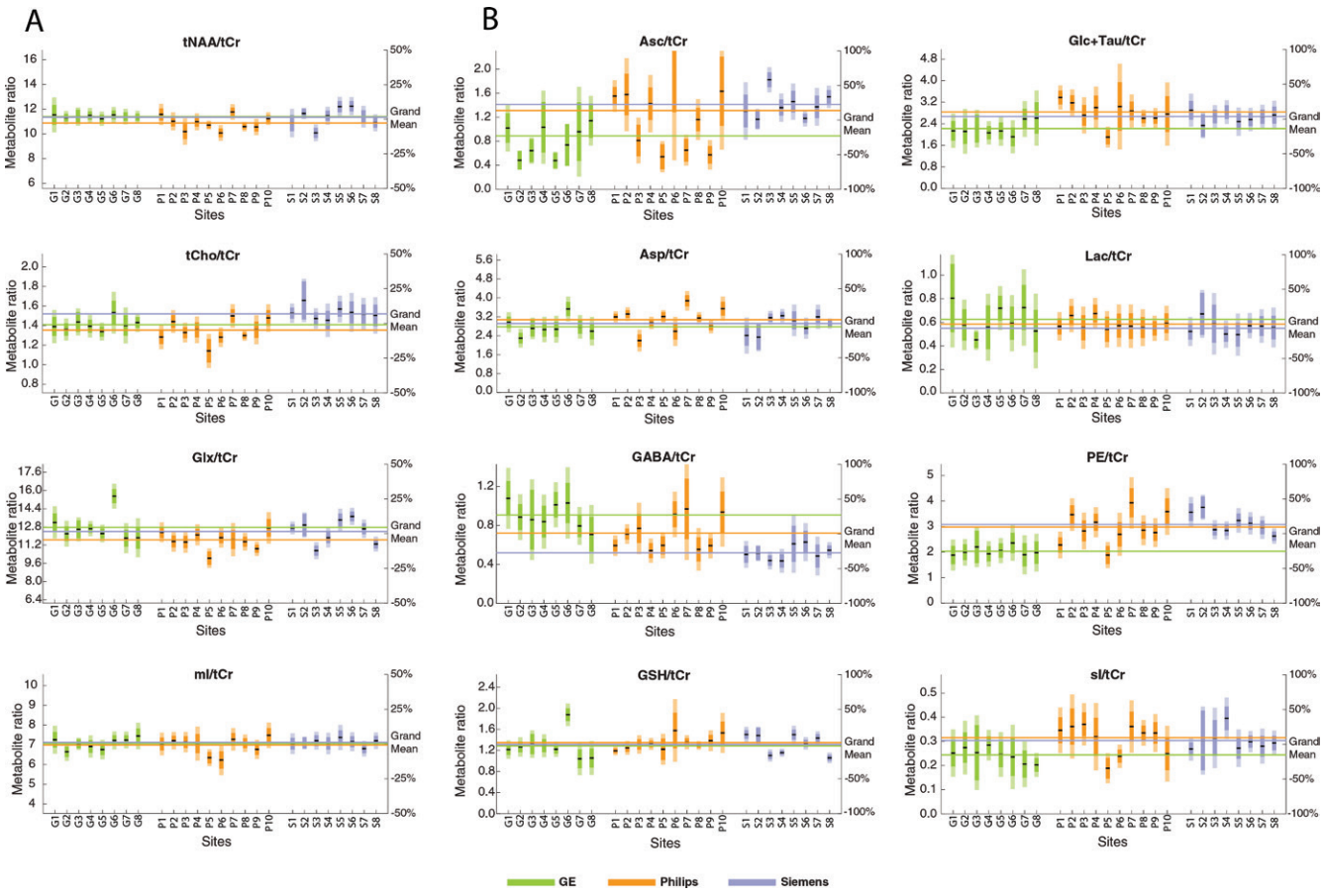

Figure 4: Graphs show metabolite ratios to total creatine (tCr) shown by site and vendor. Black lines represent mean, darker areas represent 95% confidence intervals, and tinted areas represent ±1 standard deviation. Color-coded horizontal lines represent vendor-specific mean of plotted metabolite. *A*, Major metabolite signals: total *N*-acetylaspartate (NAA), total choline (tCho), myo-inositol (mI), and glutamate and glutamine (Glx) (plotted on range of ±50% of their grand mean). *B*, Smaller signals: ascorbate (Asc), aspartate (Asp), γ-aminobutyric acid (GABA), glucose (Glc) and taurine (Tau), glutathione (GSH), lactate (Lac), phosphoethanolamine (PE), and scyllo-inositol (sI) (plotted on range of ±100% of their grand mean).

one metabolite (lactate; P_{boot} = .20) with site-level variance ranging from 3% up to 44% of total data variance. The remaining 50%–83% of the total variance was accounted for by interindividual differences, which included both actual biologic differences and participant-to-participant measurement error.

Results of the linear mixed-effects modeling are summarized in Table E6 (online). The linear mixed-effects modeling showed the effects of vendor on total choline/tCr ($P_{boot} < .001$), γ-aminobutyric acid/tCr ($P_{boot} < .001$), phosphoethanolamine/tCr ($P_{boot} < .001$), scyllo-inositol/tCr (P_{boot} = .03), and glucose and taurine/tCr (P_{boot} = .003) but not on mI/tCr ($P_{boot} > .90$), total NAA/tCr (P_{boot} = .13), Glx/tCr (P_{boot} = .11), ascorbate/tCr (P_{boot} = .08), aspartate/tCr ($P_{boot} > .90$), glutathione/tCr ($P_{boot} > .90$), or lactate/tCr (P_{boot} = .28). There was an effect of site on all metabolites (all $P_{boot} < .02$) except for lactate/tCr (P_{boot} = .20).

The conditional linear mixed-effects modeling showed an effect of SNR on ascorbate/tCr ($P_{boot} < .001$), glutathione/tCr ($P_{boot} < .001$), and mI/tCr (P_{boot} = .02) measures. Linewidth was related to aspartate/tCr ($P_{boot} < .001$), γ-aminobutyric acid/tCr ($P_{boot} < .001$), glutathione/tCr (P_{boot} = .05), phosphoethanolamine/tCr (P_{boot} = .002), and Glx/tCr (P_{boot} = .007). No metabolites showed an age effect except for lactate/tCr (P_{boot} = .007). Sex differences were observed only for ascorbate/tCr (P_{boot} = .03) and total choline/tCr (P_{boot} = .003).

Discussion

We demonstrated that short-echo-time point-resolved spectroscopy (PRESS) MR spectroscopy of the human brain performed at 3.0 T can quantify eight different metabolites in all 293 participants based on the defined quality exclusion criteria in a 27-mL voxel and approximately 2-minute scan time. Our reported metabolite ratios are in agreement with previously published values (21–23). Uncertainty estimates (ie, Cramér-Rao lower bounds [CRLBs]) of the major metabolites (ie, glutamate and glutamine [Glx], myo-inositol [mI], total choline, total creatine [tCr], and total *N*-acetylaspartate [NAA]) were under 5% in all data sets, consistent with prior studies that have also reported less than 5% CRLBs for these compounds at 3.0 T (24). Furthermore, despite no effort being made to standardize the acquisition beyond harmonization of relatively basic parameters (repetition time, echo time, voxel size, and scan time), there was no vendor effect observed for seven of the 12 metabolite-to-tCr ratios that were reported, including the major metabolites total NAA, Glx, and mI, as

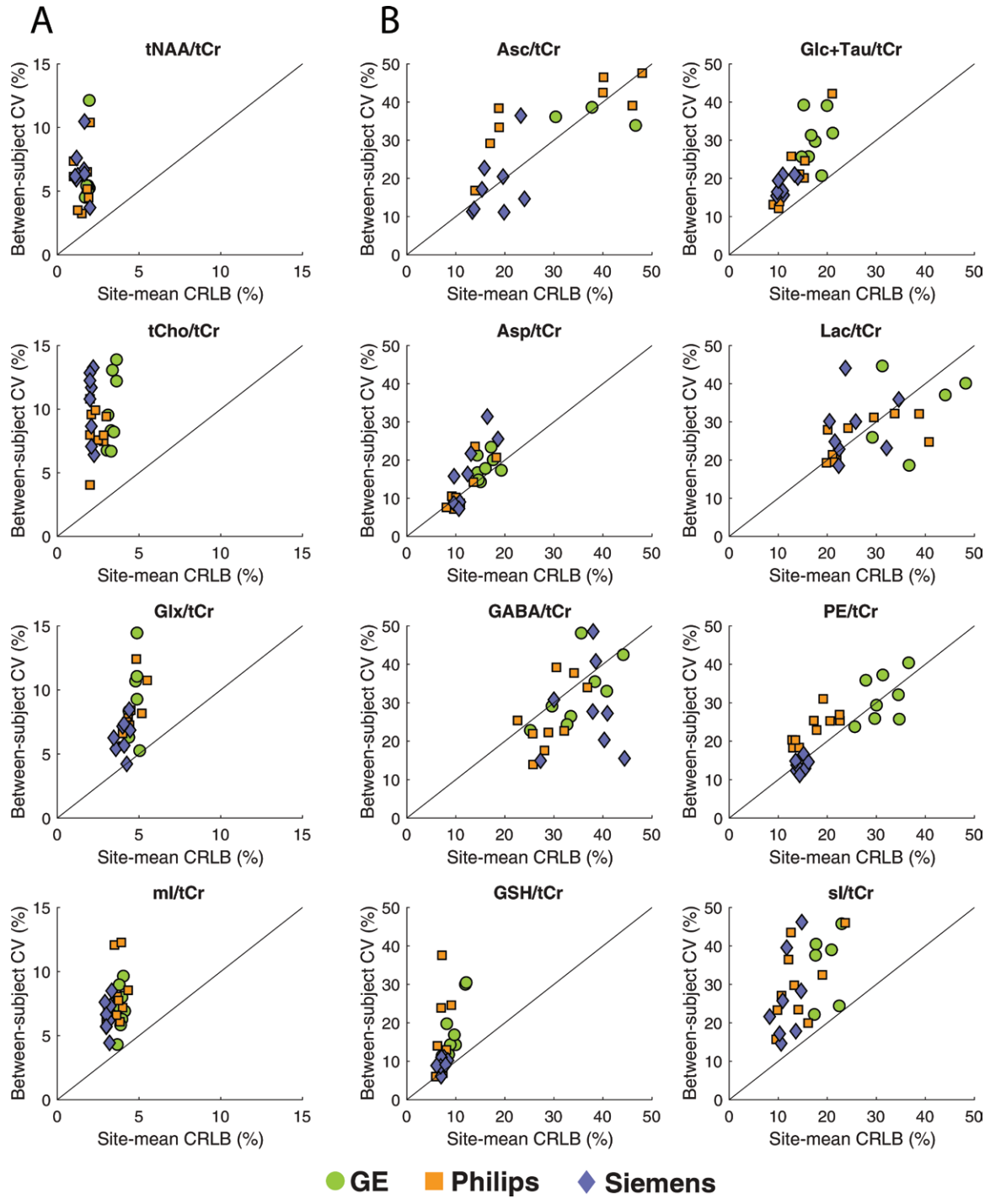

Figure 5: Graphs show between-participant coefficient of variation plotted against site-mean Cramér-Rao lower bounds (CRLBs) (error of fitting) for reported metabolite ratios to total creatine (tCr) displayed for, *A*, four major metabolites with lower CRLBs: total *N*-acetylaspartate (tNAA), total choline (tCho), myo-inositol (mI), and glutamate and glutamine (Glx). *B*, Smaller signals with higher CRLBs. Black line is identity line. Color-coded by vendors. Asc = ascorbate, Asp = aspartate, GABA = γ-aminobutyric acid, Glc = glucose, GSH = glutathione, Lac = lactate, PE = phosphoethanolamine, sI = scyllo-inositol, Tau = taurine.

well as ascorbate, aspartate, lactate, and glutathione among the smaller resonances.

Interestingly, there was a between-vendor difference of 16% for total choline, which is somewhat surprising given the lack of difference for the other major metabolite resonances. We found a vendor effect for four other metabolites (scyllo-inositol, phosphoethanolamine, glucose, and taurine) and one macromolecular signal (MM17). All these metabolites occur in a region of the spectrum (approximately 3.2 ppm to approximately 3.4 ppm) that is heavily overlapped with a number of multiplet signals. This vendor-level variability is, therefore, most likely driven by the ability of the spectral fitting algorithm to distinguish between these heavily overlapped resonances (25) and is influenced by the vendor-specific prior knowledge available, rather than by intrinsic

between-vendor spectral differences per se. Consistent with this, resonances without substantial overlap (eg, macromolecules or lactate) or those that have at least one dominant peak with minimal overlap (total NAA at 2.01 ppm, creatine and phosphocreatine at 3.03 ppm, Glx at 3.75 ppm, and mI at 3.52 ppm) were less affected by vendor-specific effects. Site-specific differences in methodology were reflected in higher contribution of site effect in total variance of most metabolites, including the major metabolites that ranged from approximately 15% for total choline and mI up to approximately 44% for Glx. This effect needs to be considered in future multisite studies; however, it may be substantially minimized by standardization of spectroscopic sequences.

Multiple technical factors influence the appearance and quality of brain MR spectra. Linewidths reflect the success of the shimming routine used, which was not standardized between sites in our study. Our relatively narrow and consistent linewidths are similar to those reported in the literature (21,24). Our data suggest that the choice of shimming method does not influence results for the midparietal brain region (which is relatively distant from magnetic susceptibility effects) (26). SNRs) depend on many factors, including radiofrequency coils used, voxel size, and pulse sequence efficiency. In our study, SNR was higher for Siemens scanners, which can be attributed to differences in how the width of the slice-selective pulses are defined by the vendors (27) (ie, the Siemens data were collected with larger actual voxel volumes compared with the other scanners, due to differences in the profiles of the slice selective pulses used for spatial localization). Although linewidth and SNR have an impact on quantification accuracy and precision (28), SNR and linewidth were not major factors influencing the variance of our data because of the large voxel size and favorable brain region used.

Importantly, we customized our analyses for each vendor. LCModel basis sets were customized to account for between-vendor differences in the PRESS sequence (ie, timing of the radiofrequency pulses and full spatial simulations of the refocusing pulse profiles). Four sites equipped with GE scanners used PRESS sequences with slightly different interpulse timings, spectral bandwidth, and number of acquired points, so we created a separate basis set for these sites.

As was the case for the shimming routine, the method of water suppression was not standardized. A variety of water suppression modules are available (29), and different scanners used different approaches. In addition, the bandwidth of the water suppression pulses was not standardized, which influenced spectral appearance near the water peak. The mI peak at 4.05 ppm was suppressed by the water suppression pulses in data sets acquired by using GE scanners and partially in data sets acquired by using Philips scanners. To a smaller extent, this effect was also observed with creatine and phosphocreatine at 3.9 ppm. To avoid this impacting spectral quantitation, the 4.1-ppm mI peak was excluded from the LCModel analysis by limiting the spectral range to 0.5–4.0 ppm, and the correction term (CrCH2) was included in the basis set to account for effects on creatine and phosphocreatine at 3.9 ppm.

Outer-volume suppression pulses were implemented in combination with PRESS localization on some scanners but not others. Outer-volume suppression helps to improve spatial localization by suppressing unwanted signals from outside the voxel, especially those from pericranial lipids that can complicate spectral analysis. We had to exclude three data sets acquired by using Siemens scanners due to lipid contamination, two of which did not include use of such pulses.

Finally, CRLBs of the major metabolites were substantially lower compared with the between-participant coefficients of variation. This has previously been suggested to reflect the dominance of interparticipant physiologic or measurement variance over the error in spectral fitting (17,30). Between-participant coefficients of variation and CRLBs were more similar for the lower-concentration metabolites. Thus, the contribution of the modeling error to between-participant differences cannot be neglected for these compounds.

Our study had several limitations. It is likely that voxel position varied slightly from participant to participant, because voxels were placed manually by different operators at each site. In addition, the introduction of a measured macromolecular spectrum into a spectral quantification (31,32) would potentially remove some of the fitting variability most notably within the range from 3–4 ppm, as the chosen macromolecular model does not cover this region.

In conclusion, our results are encouraging for the implementation of MR spectroscopy in large multisite studies of major metabolites using 3.0-T MR scanners from different vendors and also for allowing the quantitative comparison of spectra recorded at different sites (eg, for diagnostic purposes) to be more readily compared. Although single-site and single-vendor studies are ideal in minimizing variance of MR spectroscopy data, in many instances these are not feasible because it is impossible to recruit sufficient numbers of patients at individual sites. An ideal future study would image participants at all sites and might include imaging of a subset of volunteers across multiple sites to minimize between-participant variance while leaving between-site and between-vendor variance to be investigated.

Acknowledgments: I.D.W. and N. Hoggard thank the Wellcome Trust, the National Institute for Health Research Sheffield Biomedical Research Center, and J. Bigley of the University of Sheffield MRI Unit for her assistance with data acquisition.

Complete list of authors: Michal Považan, PhD; Mark Mikkelsen, PhD; Adam Berrington, PhD; Pallab K. Bhattacharyya, PhD; Maiken K. Brix, MD; Pieter F. Buur, PhD; Kim M. Cecil, PhD; Kimberly L. Chan, PhD; David Y.T. Chen, MD; Alexander R. Craven, MS; Koen Cuypers, PhD; Michael Dacko, PhD; Niall W. Duncan, PhD; Ulrike Dydak, PhD; David A. Edmondson, PhD; Gabriele Ende, PhD; Lars Ersland, PhD; Megan A. Forbes, PhD; Fei Gao, PhD; Ian Greenhouse, PhD; Ashley D. Harris, PhD; Naying He, BS; Stefanie Heba, PhD; Nigel Hoggard, MD; Tun-Wei Hsu, BS; Jacobus F. A. Jansen, PhD; Alayar Kangarlu, PhD; Thomas Lange, PhD; R. Marc Lebel, PhD; Yan Li, PhD; Chien-Yuan E. Lin, PhD; Jy-Kang Liou, PhD; Jiing-Feng Lirng, MD; Feng Liu, PhD; Joanna R. Long, PhD; Ruoyun Ma, PhD; Celine Maes, MS; Marta Moreno-Ortega, PhD; Scott O. Murray, PhD; Sean Noah, BA; Ralph Noeske, PhD; Michael D. Noseworthy, PhD; Georg Oeltzschner, PhD; Eric C. Porges, PhD; James J. Prisciandaro, PhD; Nicolaas A. J. Puts, PhD; Timothy P. L. Roberts, PhD; Markus Sack, PhD; Napapon Sailasuta, PhD; Muhammad G. Saleh, PhD; Michael-Paul Schallmo, PhD; Nicholas Simard, MS; Diederick Stoffers, PhD; Stephan P. Swinnen, PhD; Martin Tegenthoff, MD; Peter Truong, MS; Guangbin Wang, MD; Iain D. Wilkinson, PhD; Hans-Jörg Wittsack, PhD; Adam J. Woods, PhD; Hongmin Xu, PhD; Fuhua Yan, MD; Chencheng Zhang, MD; Vadim Zipunnikov, PhD; Helge J. Zöllner, PhD; Richard A.E. Edden, PhD; and Peter B. Barker, DPhil.

Author affiliations continued: Department of Radiology, University of Calgary, Calgary, Canada (A.D.H.); Department of Radiology, Ruijin Hospital, Shanghai

Jiao Tong University School of Medicine, Shanghai, China (N. He, Y.L., H.X., F.Y.); Department of Neurology, BG University Hospital Bergmannsheil, Bochum, Germany (S.H., M.T.); Academic Unit of Radiology, University of Sheffield, Sheffield, England (N. Hoggard, I.D.W.); Department of Radiology, Taipei Veterans General Hospital, National Yang-Ming University School of Medicine, Taipei, Taiwan (T.W.H., J.K.L., J.F.L.); Department of Radiology, Maastricht University Medical Center, Maastricht, the Netherlands (J.F.A.J.); Department of Psychiatry, Columbia University, New York, NY (A.K.. M.M.O.); New York State Psychiatric Institute, New York, NY (A.K., F.L.); GE Healthcare, Calgary, Canada (R.M.L.); GE Healthcare, Taipei, Taiwan (C.Y.E.L.); Department of Biochemistry and Molecular Biology, University of Florida, Gainesville, FL (J.R.L.); National High Magnetic Field Laboratory, Gainesville, FL (J.R.L.); Center for Magnetic Resonance Research, Department of Radiology, University of Minnesota, Minneapolis, MN (R.M.); Department of Psychology, University of Washington, Seattle, WA (S.O.M., M.P.S.); Center for Mind and Brain, University of California, Davis, Davis, CA (S.N.); GE Healthcare, Berlin, Germany (R.N.); Department of Electrical and Computer Engineering, McMaster University, Hamilton, Canada (M.D.N.); Department of Psychiatry and Behavioral Sciences, Medical University of South Carolina, Charleston, SC (J.J.P.); Department of Radiology, Children's Hospital of Philadelphia, Philadelphia, PA (T.P.L.R.); Research Imaging Centre, Centre for Addiction and Mental Health, Toronto, Canada (N. Sailasuta, P.T.); Department of Psychiatry, University of Toronto, Toronto, Canada (N. Sailasuta); Department of Psychiatry and Behavioral Sciences, University of Minnesota, Minneapolis, MN (M.P.S.); School of Biomedical Engineering, McMaster University, Hamilton, Canada (N. Simard); Leuven Brain Institute (LBI), KU Leuven, Leuven, Belgium (S.P.S.); Department of Diagnostic and Interventional Radiology, Medical Faculty, Heinrich-Heine-University, Duesseldorf, Germany (H.J.W., H.J.Z.); Department of Functional Neurosurgery, Ruijin Hospital, Shanghai Jiao Tong University School of Medicine, Shanghai, China (C.Z.); Department of Biostatistics, Johns Hopkins Bloomberg School of Public Health, Baltimore, MD (A.Y.); and Institute of Clinical Neuroscience and Medical Psychology, Medical Faculty, Heinrich-Heine-University, Duesseldorf, Germany (H.J.Z.).

Author contributions: Guarantors of integrity of entire study, M.P., M.M., T.W.H., J.K.L., M.M.O., N.A.J.P., N. Sailasuta, G.W., P.B.B.; study concepts/study design or data acquisition or data analysis/interpretation, all authors; manuscript drafting or manuscript revision for important intellectual content, all authors; approval of final version of submitted manuscript, all authors; agrees to ensure any questions related to the work are appropriately resolved, all authors; literature research, M.P., L.E., J.K.L., J.R.L., M.M.O., R.N., M.D.N., N.A.J.P., M.T., G.W., I.D.W., H.X., F.Y., C.Z., R.A.E.E., P.B.B.; clinical studies, D.Y.T.C., F.G., Y.L., C.Y.E.L., J.K.L., J.J.P., N. Sailasuta, G.W., I.D.W., H.X., F.Y., C.Z.; experimental studies, M.P., M.M., A.B., P.K.B., K.M.C., K.L.C., A.R.C., K.C., M.D., N.W.D., U.D., G.E., L.E., I.G., A.D.H., N. He, S.H., N. Hoggard, A.K., T.L., R.M.L., J.K.L., J.F.L., J.R.L., R.M., C.M., M.M.O., S.O.M., M.D.N., G.O., E.C.P., J.J.P., N.A.J.P., T.P.L.R., M.S., M.P.S., N. Simard, D.S., S.P.S., M.T., P.T., G.W., H.J.W., H.X., C.Z., R.A.E.E.; statistical analysis, M.P., M.M., M.K.B., J.K.L., G.W., H.X., F.Y., C.Z.; and manuscript editing, M.P., M.M., A.B., P.K.B., M.K.B., K.M.C., K.L.C., K.C., U.D., G.E., L.E., A.D.H., N. He, S.H., N. Hoggard, T.W.H., J.F.A.J., A.K., J.K.L., J.R.L., M.M.O., S.O.M., M.D.N., G.O., E.C.P., J.J.P., N.A.J.P., T.P.L.R., M.S., M.G.S., M.P.S., M.T., G.W., I.D.W., H.J.W., A.J.W., H.X., F.Y., C.Z., V.Z., R.A.E.E., P.B.B.

Disclosures of Conflicts of Interest: **M.P.** disclosed no relevant relationships. **M.M.** disclosed no relevant relationships. **A.B.** disclosed no relevant relationships. **P.K.B.** disclosed no relevant relationships. **M.K.B.** disclosed no relevant relationships. **P.F.B.** disclosed no relevant relationships. **K.M.C.** Activities related to the present article: disclosed no relevant relationships. Activities not related to the present article: is a consultant for and received clinical trial contract award from Lumos Pharma; is employed by University of Cincinnati College of Medicine; has grants/grants pending with National Institutes of Health (NIH); received payment for lectures including service on speakers bureaus at State of New Hampshire Health Home Conference; is study section member at NIH Center for Scientific Review; was guest speaker at Kentucky Wesleyan College. Activities not related to the present article: disclosed no relevant relationships. Other relationships: disclosed no relevant relationships. **K.L.C.** disclosed no relevant relationships. **D.Y.T.C.** disclosed no relevant relationships. **A.R.C.** Activities related to the present article: disclosed no relevant relationships. Activities not related to the present article: holds stock/stock options in NordicNeuroLab. Other relationships: disclosed no relevant relationships. **K.C.** disclosed no relevant relationships. **M.D.** disclosed no relevant relationships. **N.W.D.** disclosed no relevant relationships. **U.D.** disclosed no relevant relationships. **D.A.E.** disclosed no relevant relationships. **G.E.** disclosed no relevant relationships. **L.E.** disclosed no relevant relationships. **M.A.F.** disclosed no relevant relationships. **F.G.** disclosed no relevant relationships. **I.G.** disclosed no relevant relationships. **A.D.H.** Activities related to the present article: institution received funds through a subcontract of the NIH grant awarded to Richard Edden to offset MRI scanning costs that was performed at University of Calgary. Activities not related to the present article: disclosed no relevant relationships. Other relationships: disclosed no relevant relationships. **N.He** disclosed no relevant relationships. **S.H.** Activities related to the present article: institution received grant from German Research Foundation (Sonderforschungsbereich 874, Project no. 122679504). Activities not related to the present article: disclosed no relevant relationships. Other relationships: disclosed no relevant relationships. **N. Hoggard** disclosed no relevant relationships. **T.W.H.** disclosed no relevant relationships. **J.F.A.J.** disclosed no relevant relationships. **A.K.** disclosed no relevant relationships. **T.L.** disclosed no relevant relationships. **R.M.L.** Activities related to the present article: disclosed no relevant relationships. Activities not related to the present article: is employed by and holds stock/stock options in GE Healthcare. Other relationships: disclosed no relevant relationships. **Y.L.** disclosed no relevant relationships. **C.Y.E.L.** Activities related to the present article: disclosed no relevant relationships. Activities not related to the present article: is employed by GE Healthcare Taiwan. Other relationships: disclosed no relevant relationships. **J.K.L.** disclosed no relevant relationships. **J.F.L.** disclosed no relevant relationships. **F.L.** disclosed no relevant relationships. **J.R.L.** Activities related to the present article: disclosed no relevant relationships. Activities not related to the present article: received payment for travel/accommodations/meeting expenses unrelated to activities listed from Philips and Siemens. Other relationships: disclosed no relevant relationships. **R.M.** disclosed no relevant relationships. **C.M.** disclosed no relevant relationships. **M.M.O.** disclosed no relevant relationships. **S.O.M.** disclosed no relevant relationships. **S.N.** disclosed no relevant relationships. **R.N.** Activities related to the present article: disclosed no relevant relationships. Activities not related to the present article: is employed by GE Healthcare. Other relationships: disclosed no relevant relationships. **M.D.N.** disclosed no relevant relationships. **G.O.** disclosed no relevant relationships. **E.C.P.** Activities related to the present article: disclosed no relevant relationships. Activities not related to the present article: is board member of Evren Technologies; is employed by University of Florida. Other relationships: disclosed no relevant relationships. **J.J.P.** Activities related to the present article: disclosed no relevant relationships. Activities not related to the present article: is a consultant for Laboratorio Farmaceutico CT Srl. Other relationships: disclosed no relevant relationships. **N.A.J.P.** Activities related to the present article: disclosed no relevant relationships. Activities not related to the present article: is employed by the Johns Hopkins University School of Medicine; has grants/grants pending with NIH/Eunice Kennedy Shriver National Institute of Child Health and Human Development. Other relationships: disclosed no relevant relationships. **T.P.L.R.** Activities related to the present article: disclosed no relevant relationships. Activities not related to the present article: is board member of CTF and MEG; is a consultant for Avexis, Ricoh, and Spago; has grants/grants pending with NIH; has patents (planned, pending, or issued) with Elekta Oy; holds stock/stock options in Prism Clinical Imaging; has consulting agreement with Acadia. Other relationships: disclosed no relevant relationships. **M.S.** disclosed no relevant relationships. **N. Sailasuta** Activities related to the present article: disclosed no relevant relationships. Activities not related to the present article: collaborated with Centre for Addiction and Mental Health. Other relationships: disclosed no relevant relationships. **M.G.S.** disclosed no relevant relationships. **M.P.S.** disclosed no relevant relationships. **N. Simard** disclosed no relevant relationships. **D.S.** disclosed no relevant relationships. **S.P.S.** disclosed no relevant relationships. **M.T.** Activities related to the present article: disclosed no relevant relationships. Activities not related to the present article: is employed by Ruhr University; has grants/grants pending with DFG and DGUV; received payment for lectures including service on speakers bureaus and payment for travel/accommodations/meeting expenses unrelated to activities listed from Novartis; received payment for development of educational presentations from DGUV. Other relationships: disclosed no relevant relationships. **P.T.** disclosed no relevant relationships. **G.W.** disclosed no relevant relationships. **I.D.W.** disclosed no relevant relationships. **H.J.W.** disclosed no relevant relationships. **A.J.W.** disclosed no relevant relationships. **H.X.** disclosed no relevant relationships. **F.Y.** disclosed no relevant relationships. **C.Z.** disclosed no relevant relationships. **V.Z.** disclosed no relevant relationships. **H.J.Z.** Activities related to the present article: disclosed no relevant relationships. Activities not related to the present article: is employed by the Institute for Clinical Neuroscience and Medical Psychology (Germany). Other relationships: disclosed no relevant relationships. **R.A.E.E.** Activities related to the present article: disclosed no relevant relationships. Activities not related to the present article: has grants/grants pending with Siemens Medical Systems. Other relationships: disclosed no relevant relationships. **P.B.B.** Activities related to the present article: disclosed no relevant relationships. Activities not related to the present article: has grants/grants pending with NIH. Other relationships: disclosed no relevant relationships.

References

1. Barker PB, Bizzi A, De Stefano N, Gullapalli RP, Lin DDM. Clinical MR Spectroscopy: Techniques and applications. Cambridge, England: Cambridge University Press, 2009.
2. Öz G, Alger JR, Barker PB, et al. Clinical proton MR spectroscopy in central nervous system disorders. Radiology 2014;270(3):658–679.
3. Bottomley P. Selective volume method for performing localized NMR spectroscopy. US Patent 4,480,228. 1984.
4. Scheenen TWJ, Klomp DWJ, Wijnen JP, Heerschap A. Short echo time 1H-MRSI of the human brain at 3T with minimal chemical shift displacement errors using adiabatic refocusing pulses. Magn Reson Med 2008;59(1):1–6.

5. Park YW, Deelchand DK, Joers JM, et al. AutoVOI: real-time automatic prescription of volume-of-interest for single voxel spectroscopy. Magn Reson Med 2018;80(5):1787–1798.
6. Mescher M, Merkle H, Kirsch J, Garwood M, Gruetter R. Simultaneous in vivo spectral editing and water suppression. NMR Biomed 1998;11(6):266–272.
7. Mikkelsen M, Barker PB, Bhattacharyya PK, et al. Big GABA: Edited MR spectroscopy at 24 research sites. Neuroimage 2017;159:32–45.
8. Mikkelsen M, Rimbault DL, Barker PB, et al. Big GABA II: Water-referenced edited MR spectroscopy at 25 research sites. Neuroimage 2019;191(3):537–548.
9. Považan M, Strasser B, Hangel G, et al. Automated routine for MRSI data processing. In: Proceedings 2nd TRANSACT Meeting-Quality Issues in Clinical MR Spectroscopy. Bern, Switzerland: University and Inselspital; 2014.
10. Simpson R, Devenyi GA, Jezzard P, Hennessy TJ, Near J. Advanced processing and simulation of MRS data using the FID appliance (FID-A)-An open source, MATLAB-based toolkit. Magn Reson Med 2017;77(1):23–33.
11. Brown MA. Time-domain combination of MR spectroscopy data acquired using phased-array coils. Magn Reson Med 2004;52(5):1207–1213.
12. Near J, Edden R, Evans CJ, Paquin R, Harris A, Jezzard P. Frequency and phase drift correction of magnetic resonance spectroscopy data by spectral registration in the time domain. Magn Reson Med 2015;73(1):44–50.
13. Provencher SW. Estimation of metabolite concentrations from localized in vivo proton NMR spectra. Magn Reson Med 1993;30(6):672–679.
14. Berrington A, Voets NL, Plaha P, et al. Improved localisation for 2-hydroxyglutarate detection at 3T using long-TE semi-LASER. Tomography 2016;2(2):94–105.
15. Tkáč I. Refinement of simulated basis set for LCModel analysis [abstr]. In: Proceedings of the Sixteenth Meeting of the International Society for Magnetic Resonance in Medicine. Berkeley, Calif: International Society for Magnetic Resonance in Medicine, 2008; 1624.
16. Govind V, Young K, Maudsley AA. Corrigendum: proton NMR chemical shifts and coupling constants for brain metabolites. Govindaraju V, Young K, Maudsley AA, NMR Biomed. 2000; 13: 129-153. NMR Biomed 2015;28(7):923–924.
17. Tkáč I, Oz G, Adriany G, Uğurbil K, Gruetter R. In vivo 1H NMR spectroscopy of the human brain at high magnetic fields: metabolite quantification at 4T vs. 7T. Magn Reson Med 2009;62(4):868–879.
18. R Core Team. R: A Language and Environment for Statistical Computing. Vienna, Austria: R Foundation for Statistical Computing, 2018. https://www.r-project.org.
19. Halekoh U, Højsgaard S. A Kenward-Roger Approximation and Parametric Bootstrap Methods for Tests in Linear Mixed Models - The R Package pbkrtest. J Stat Softw 2014;59(9):1–32.
20. Holm S. A Simple Sequentially Rejective Multiple Test Procedure. Scand J Stat 1979;6(2):65–70.
21. Baker EH, Basso G, Barker PB, Smith MA, Bonekamp D, Horská A. Regional apparent metabolite concentrations in young adult brain measured by (1)H MR spectroscopy at 3 Tesla. J Magn Reson Imaging 2008;27(3):489–499.
22. Ross B, Bluml S. Magnetic resonance spectroscopy of the human brain. Anat Rec 2001;265(2):54–84.
23. Kirov II. Concentration Ranges of Common Metabolites Detected by MRS in Healthy Human Tissue. In: Bottomley PA, Griffiths JR, eds. Handbook of Magnetic Resonance Spectroscopy In Vivo: MRS Theory, Practice and Applications. Chichester, England: Wiley, 2016; 1057–1059.
24. Pradhan S, Bonekamp S, Gillen JS, et al. Comparison of single voxel brain MRS AT 3T and 7T using 32-channel head coils. Magn Reson Imaging 2015;33(8):1013–1018.
25. Hofmann L, Slotboom J, Jung B, Maloca P, Boesch C, Kreis R. Quantitative 1H-magnetic resonance spectroscopy of human brain: Influence of composition and parameterization of the basis set in linear combination model-fitting. Magn Reson Med 2002;48(3):440–453.
26. Li S, Dardzinski BJ, Collins CM, Yang QX, Smith MB. Three-dimensional mapping of the static magnetic field inside the human head. Magn Reson Med 1996;36(5):705–714.
27. Saleh MG, Rimbault D, Mikkelsen M, et al. Multi-vendor standardized sequence for edited magnetic resonance spectroscopy. Neuroimage 2019;189:425–431.
28. Bartha R. Effect of signal-to-noise ratio and spectral linewidth on metabolite quantification at 4 T. NMR Biomed 2007;20(5):512–521.
29. Lei H, Xin L, Gruetter R, Mlynárik V. Localized Single-Voxel Magnetic Resonance Spectroscopy, Water Suppression, and Novel Approaches for Ultrashort Echo-Time Measurements. In: Stagg CJ, Rothman DL, eds. Magnetic Resonance Spectroscopy. Oxford, England: Academic Press, 2013; 15–30.
30. Deelchand DK, Adanyeguh IM, Emir UE, et al. Two-site reproducibility of cerebellar and brainstem neurochemical profiles with short-echo, single-voxel MRS at 3T. Magn Reson Med 2015;73(5):1718–1725.
31. Schaller B, Xin L, Cudalbu C, Gruetter R. Quantification of the neurochemical profile using simulated macromolecule resonances at 3 T. NMR Biomed 2013;26(5):593–599.
32. Birch R, Peet AC, Dehghani H, Wilson M. Influence of macromolecule baseline on ^{1}H MR spectroscopic imaging reproducibility. Magn Reson Med 2017;77(1):34–43.